


A.B. SUGIHARTO
C.M. JOHNSON
H.B. DE AGUIAR
L. ALLOATTI
S. ROKE 

Generation and application of high power femtosecond pulses in the vibrational fingerprint region

Max Planck Institute for Metals Research, Heisenbergstrasse 3, 70569 Stuttgart, Germany

Received: 16 October 2007/Revised version: 25 February 2008
Published online: 8 April 2008 • © The Author(s) 2008

ABSTRACT We present a novel high power femtosecond infrared laser source, based on a three-stage chirped-pulse amplification scheme. Owing to the high power output of the Ti:sapphire amplifiers, it becomes routinely possible to produce femtosecond infrared laser pulses in the wavelength region of 2.6–20 μm with minimum pulse energies of 15 μJ , to our knowledge roughly an improvement of an order of magnitude. With such pulses we have performed femtosecond second-order nonlinear optical surface spectroscopy in the fingerprint region. We have probed the skeletal modes of the first few monolayers of a polymer/air interface in a femtosecond vibrational sum frequency generation experiment. This development opens up new possibilities to investigate surface structures and dynamics of, e.g., organo-metallic compounds, proteins, and peptides.

PACS 42.65.-k; 68.35.-Ja; 82.35.Ps

1 Introduction

In nature, many energy levels lie in the low frequency region of the mid-infrared region (8–20 μm). Examples are vibrational modes associated with the three-dimensional structure of organic compounds [1], metal-adsorbate interactions [2] and transitions in semiconductors [3]. Probing the structure and dynamics of these energy levels will open up new avenues in research areas related to three-dimensional structure determination of polymers, peptides and proteins in bulk or at interfaces, surface science and catalysis as well as the design and application of semi-conductor devices. Until now, most studies that utilize low frequency mid-infrared radiation rely on incoherent light sources. Routine access to femtosecond low frequency infrared pulses (with significant power) would mean a significant improvement in the above mentioned research areas, since it allows for the application of nonlinear optics (e.g., vibrational sum frequency generation to probe three-dimensional interfacial structures), vibrational dynamics studies [4, 5], two-dimensional spectroscopy [6] and interfacial time domain [7] and pump-probe studies [8–10].

Femtosecond pulses with wavelengths up to 20 μm have been reported [11–14]. However, the energy of these pulses is only one to a few μJ . Such low intensities significantly complicate the experiments in this infrared regime. Consequently,

the number of experiments using them remains limited to only a few (e.g., [15–17]). As an example, surface signals of phospholipid molecules down to 10 μm have been observed in a femtosecond vibrational sum frequency experiment, but the data shows very low signal to noise ratios [17]. Table-top picosecond systems with a similar output power have been reported as well [18, 19]. Higher output power (of ~ 60 mW), combined with pulse durations in the range 500 fs–2 ps can be obtained in the wavelength range from 5 μm to 50 μm with a free electron laser source [20–22]. This is, however, not a table-top source but a facility. Thus, to date (as far as we know) femtosecond pulse energies in the vibrational fingerprint region are insufficient or insufficiently available to routinely observe second-order nonlinear optical effects.

In this article, we show that we have obtained femtosecond infrared pulses in the frequency range of 2.6–20 μm , with (minimum) pulse energies of 15 μJ , to our knowledge roughly a factor of ten more than is currently available from table-top sources. We show that, with this high power, we can observe (with excellent signal to noise) the skeletal modes of the first few monolayers of a biodegradable polymer film in a femtosecond vibrational sum frequency generation (VSFG) experiment.

2 Experimental

The experimental setup is depicted in Fig. 1 and consists of an oscillator (Femtolasers) that delivers pulses of 50 fs duration, at 77 MHz, with an output power of 100 mW. These pulses are stretched and amplified in a regenerative amplifier (RGA) with 4 mJ, 150 ns, 527 nm pump pulses at a repetition rate of 1 kHz. The second amplification occurs in a Ti:sapphire crystal, pumped by 12.6 mJ, 150 ns, 527 nm pulses (Quantronix). The resulting 3.8 W is then passed through a Pockel's cell to optimize pulse contrast ratio and amplified in a third stage. This stage is pumped by two Nd:YLF lasers both giving 15 mJ pump energy. The pump arms propagate in opposite directions through a Ti:sapphire crystal that is placed in a vacuum chamber (with a base pressure of 5×10^{-8} mbar). The crystal is thermally stabilized at 77 K, to minimize thermal lensing. The resulting pulse energy is 12 mJ, which is then compressed into pulses with an energy of 7.5 mJ and duration of 70 fs. Of the generated pulses 5–6.5 mJ of the energy is used to generate infrared (IR) pulses. The other fraction is shaped in a pulse shaper and used as visible (VIS) pulse with adjustable bandwidth.

✉ Fax: +49-711-6893612, E-mail: roke@mf.mpg.de

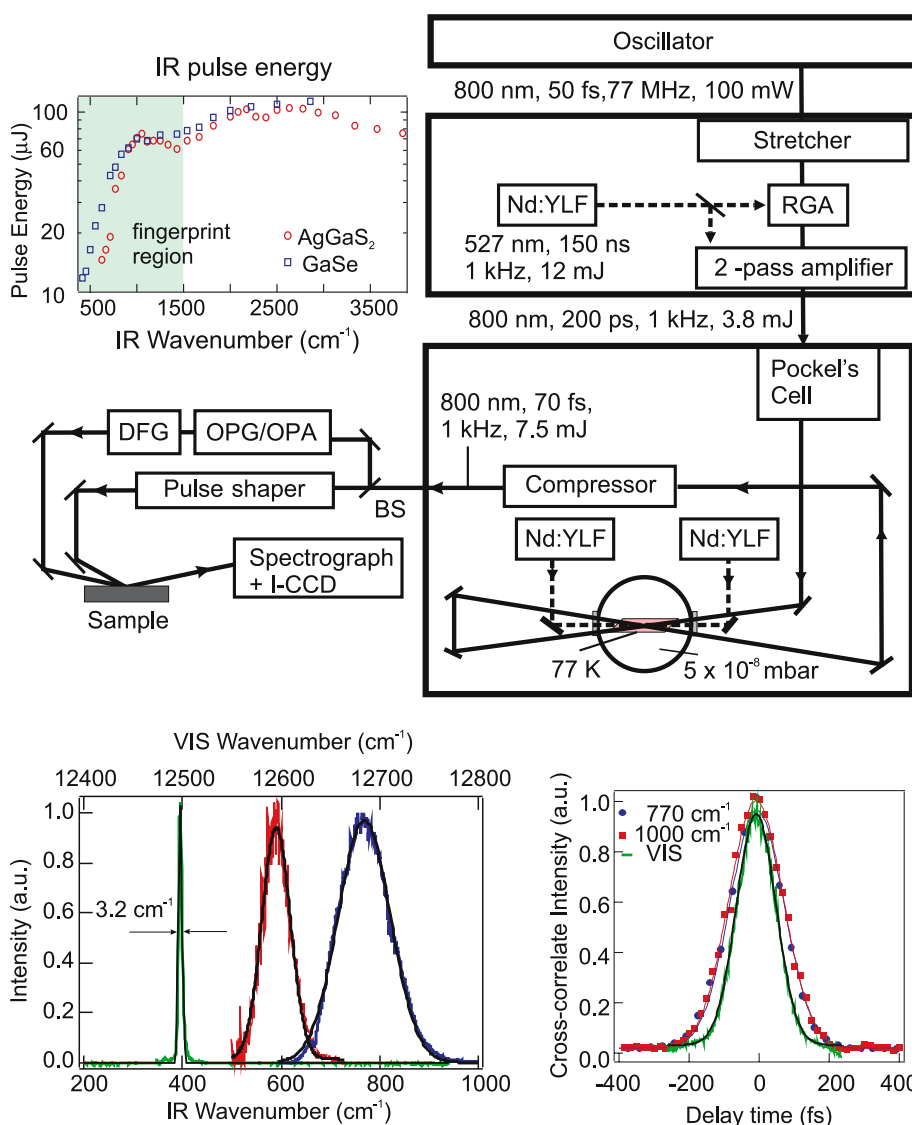


FIGURE 1 An illustration of the three stage setup for the generation of high power femtosecond 800 nm pulses. A sketch of the VSFG setup is also shown together with a plot of the infrared pulse energies as a function of IR wavenumber

FIGURE 2 Pulse characterization. *Left:* Pulses used for frequency domain SFG experiments, showing the narrow bandwidth (FWHM 3.2 cm^{-1}) visible pulse and two low frequency SFG spectra of the infrared pulses with the same visible pulse. *Right:* Cross-correlation of two infrared pulses centered at 1000 cm^{-1} ($10 \mu\text{m}$) (squares) and 770 cm^{-1} ($13 \mu\text{m}$) (circles) with a 100 fs visible pulse (intensity FWHM). The autocorrelation of the same 800 nm pulse is also shown (straight line)

To generate the IR pulses, a small portion of the energy undergoes generation of superfluorescence in a β -BBO crystal, after which it is optically parametrically amplified to tunable near infrared radiation. The obtained signal pulses ($1.1\text{--}1.6 \mu\text{m}$) are then used as a seed in another 2 mm thick β -BBO crystal, which is pumped by the remaining 800 nm pulses. The resulting $0.6\text{--}3 \text{ mJ}$ signal ($1.1\text{--}1.6 \mu\text{m}$) and idler ($1.6\text{--}2.6 \mu\text{m}$) are mixed in a DFG crystal (AgGaS_2 or GaSe), to obtain IR pulses tunable from $2.6\text{--}14 \mu\text{m}$ (AgGaS_2 , 1 mm thick) and $3.0\text{--}20 \mu\text{m}$ (GaSe , 0.46 mm thick) (Light Conversion). Figure 1 (top left panel) shows the output pulse energy (as measured with a pyroelectric detector) as a function of the IR frequency. The IR frequency itself was measured by injecting the IR pulses in the external entrance port of an FT-IR spectrometer (Bruker Vertex 70).

The resulting IR pulses were characterized in time- and frequency-domain by mixing them with characterized 800 nm pulses on a gold surface and measuring the generated sum frequency signal. In this experiment p polarized IR and VIS pulses were reflected from a gold film, and the p polarized sum frequency photons were detected. The incident an-

gles were respectively 60 and 40° with respect to the surface normal. The results are displayed in Fig. 2. For the frequency domain experiment the 800 nm pulses were shaped with a pulse shaper (consisting of a grating, a lens, a mirror and a slit). The resultant (3.2 cm^{-1} FWHM) narrow-band visible pulses were mixed with infrared pulses on a gold surface. The SFG intensity was collected as a function of frequency with a spectrometer in combination with an intensified CCD camera [20, 21, 23]. The left panel of Fig. 2 shows the result for IR pulses centered at $13 \mu\text{m}$ (770 cm^{-1}) and for pulses centered at $17 \mu\text{m}$ (600 cm^{-1}). The FWHM bandwidth of the pulses is around 125 cm^{-1} . Lower infrared frequencies can be generated, but not detected in such an SFG experiment due to the close proximity in frequency of the SFG signal with the high frequency tail of the visible pulse. (As a result the FWHM bandwidth of the pulse centered at 600 cm^{-1} appears less than it actually is.) For the time-domain experiment shown in the right panel of Fig. 2, visible pulses with a duration of 100 fs were mixed with the infrared pulses on a gold film and recorded as a function of time delay. Corresponding pulse widths in the time-domain are 130 fs for the IR

pulses. The resulting time-bandwidth product is 0.5 (assuming Gaussian pulse shapes), which is close to the Fourier limit. The time-bandwidth product could be improved by inserting optical components with appropriate dispersive characteristics [24, 25].

These measurements show we can generate femtosecond IR pulses with high power and femtosecond pulse duration in the frequency region below 1500 cm^{-1} . In this wavelength range one can expect to measure a wide variety of nonlinear optical (surface) phenomena, including the three-dimensional structure of organic compounds, metal-adsorbate interactions, and transitions in semiconductors. Our up-scaled power enables us to do such experiments with excellent signal to noise, as demonstrated below.

3 VSFG spectroscopy in the fingerprint region

As an example, we show here the measurement of the structure of the first few monolayers of the polymer/air surface of a biodegradable polymer, namely poly-(L-lactic acid) (PLLA), by performing femtosecond vibrational sum frequency spectroscopy. PLLA is used as a material for tissue regeneration and as drug carrier [26]. The three-dimensional structure of the first few monolayers at the polymer/air interface is thus extremely important for its applications.

In its crystalline form, the backbone of a PLLA polymer is organized in a helical structure (as depicted on the right side of Fig. 3). The crystalline structure of PLLA has been determined to belong to the $P2_12_12_1$ space group [27, 28]. As such, we expect both a bulk and a surface response. The bulk response appears through the second-order susceptibility elements $\chi_{xyz}^{(2)}$, $\chi_{yzx}^{(2)}$, $\chi_{zxy}^{(2)}$, $\chi_{yxz}^{(2)}$, $\chi_{xzy}^{(2)}$, $\chi_{zyx}^{(2)}$, while the surface response mainly originates from the $\chi_{xxz}^{(2)}$, $\chi_{xzx}^{(2)}$, $\chi_{zxx}^{(2)}$, $\chi_{yyz}^{(2)}$, $\chi_{zyy}^{(2)}$, and $\chi_{zzz}^{(2)}$ elements. For films with a thickness below a few microns interfacial responses can be selectively probed by using the ssp polarization combination (that consists of a combination of *s* polarized VIS and SFG beams and a *p* polarized IR beam). We have prepared the film by spin coating a solution of 0.25 wt. % poly-L lactic acid (obtained from Purac Biochem) in chloroform (Sigma-Aldrich). The spun film with a thickness of a few 100 nm, was crystallized by successive annealing at $125\text{ }^\circ\text{C}$ for 10 min [28].

Figure 3 shows frequency domain surface vibrational SFG spectra of the crystalline polymer film (top trace). The data were baseline-subtracted and normalized for acquisition time and incoming pulse energy. The spectra were fit according to the well-known formulas for the SFG intensity (see e.g., [22, 29]):

$$I_{\text{SFG}}(\omega) \propto \left| E_{\text{IR}}(\omega) \sum_n \int_{-\infty}^{\infty} \left(\chi_n^{(2)}(\omega') + \chi_{\text{NR}}^{(2)} \right) E_{\text{VIS}}(\omega' - \omega) d\omega' \right|^2, \quad (1)$$

$$\chi_{\text{NR}}^{(2)} = A_{\text{NR}} e^{i\Delta\phi}, \quad \chi_n^{(2)}(\omega) = \frac{A_n}{(\omega - \omega_{0n}) + i\Gamma_n},$$

where n refers to a vibrational mode with resonance frequency ω_{0n} and spectral half width at half maximum, Γ_n . A_{NR} repre-

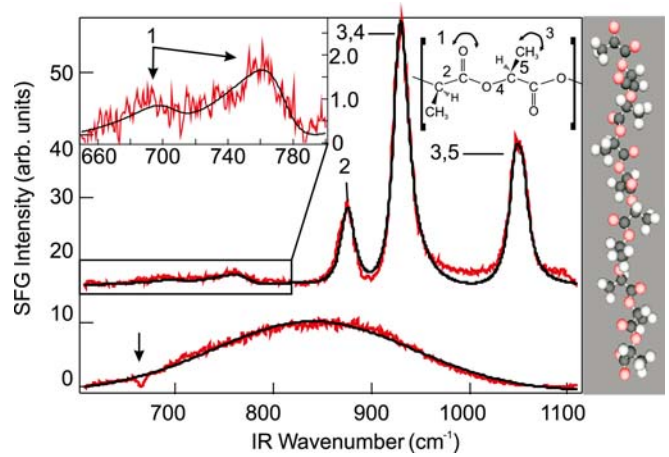


FIGURE 3 Surface vibrational SFG spectra of a crystalline PLLA film (top trace) and that of a gold film for the same IR frequency (bottom trace). The low frequency part of the spectrum displays the bending modes of the C=O groups and is enlarged in the inset. The black lines are fits to the data. The arrow in the bottom trace marks the absorbance of CO₂ in air, which can be used as an absolute measure of the frequency. The chemical structure of a PLLA monomer is also shown, together with the assignments of the observed modes in the spectrum (indicated by the numbers 1–5). A molecular modelling image of the three dimensional structure of a helical PLLA unit is also shown

sents the amplitude of the non-resonant background, and $\Delta\phi$ is the relative phase difference between the resonant and the non-resonant sum frequency fields. The solid lines in Fig. 3 are fits to the data using this equation. The fits were made using the IR pulse characteristics as obtained from the measurement on the gold film, using frequencies as close as possible to the ones reported by a normal mode analysis and an IR/Raman study on crystallized PLLA films [28]. A spectrum of the used visible pulses is shown in Fig. 2. We observe the lowest frequency modes at 704 cm^{-1} ($A = 0.14$, $\Gamma = 18$) and 773 cm^{-1} ($A = 0.21$, $\Gamma = 17.5$), which correspond to the vibrational out-of-plane and in-plane bending of the C=O group [28]. The modes at 875 cm^{-1} ($A = -0.54$, $\Gamma = 8.8$) and 929 cm^{-1} ($A = -1.3$, $\Gamma = 9.7$) represent the stretching of the C-COO bond and the rocking of the CH₃ groups in combination with the stretching of the O-CH groups, while the modes at 1047 cm^{-1} ($A = -2.5$, $\Gamma = 7.9$) and 1054 cm^{-1} ($A = -1.9$, $\Gamma = 7.4$) correspond to a mixture of CH₃ rocking and C-CH₃ stretching modes. This particular combination of skeletal mode frequencies can be correlated (through the normal mode analysis in combination with linear vibrational spectroscopy data and X-ray diffraction measurements) to a helical structure in the polymer skeleton [28, 30], as displayed in the right part of Fig. 3.

Thus, by performing femtosecond second-order nonlinear optical surface spectroscopy in the fingerprint region we can determine that PLLA chains situated at the polymer/air interface adopt a helical configuration. The vibrational modes have widths that correspond to $(1/e)$ decay times in the range of 300–750 fs and resemble the widths found for high frequency modes [7]. Therefore it is extremely likely that such time-resolved measurements can also be performed in the fingerprint region. Because low frequency modes are in general much more sensitive to the local environment we can expect to obtain useful new insights from such measurements.

4 Conclusions

In conclusion, we present a novel high power femtosecond infrared laser source, based on a three-step chirped-pulse amplification scheme. Owing to the high power of the Ti:sapphire amplifiers, it becomes possible to routinely produce femtosecond infrared laser pulses in the wavelength region of 2.6–20 μm with minimum pulse energies of 15 μJ , to our knowledge roughly an improvement of an order of magnitude. With such pulses we have performed second-order nonlinear optical surface spectroscopy in the fingerprint region. We have measured the three-dimensional backbone structure of complex biodegradable PLLA polymers at the polymer/air interface, by performing femtosecond vibrational sum frequency generation. As we have shown with the above application, it can be expected that the three-dimensional structure and dynamics of a wide range of (interfacial) systems can now be studied, including e.g., polymers, proteins, peptides and, (catalytic) metallo-organic compounds.

ACKNOWLEDGEMENTS C.M.J. acknowledges support from the Alexander von Humboldt foundation. This work is part of the research program of the Max Planck Society.

OPEN ACCESS This article is distributed under the terms of the Creative Commons Attribution Noncommercial License which permits any noncommercial use, distribution, and reproduction in any medium, provided the original author(s) and source are credited.

REFERENCES

- 1 J. McMurry, *Organic Chemistry* (Brooks/Cole Pub Co, New York, 1995)
- 2 P.W. Atkins, *Physical Chemistry* (Oxford University Press, Oxford, 1990)
- 3 T. Elsaesser, M. Woerner, *Phys. Rep.* **321**, 254 (1999)
- 4 J. Stenger, D. Madsen, P. Hamm, E.T.J. Nibbering, T. Elsaesser, *Phys. Rev. Lett.* **8702**, 027401 (2001)
- 5 A.M. Dokter, S. Woutersen, H.J. Bakker, *Proc. Nat. Acad. Sci.* **103**, 15355 (2006)
- 6 J. Bredenbeck, J. Helbing, P. Hamm, *J. Chem. Phys.* **121**, 5943 (2004)
- 7 S. Roke, A.W. Kleyn, M. Bonn, *Chem. Phys. Lett.* **370**, 227 (2003)
- 8 J. Kubota, K. Domen, *Anal. Bioanal. Chem.* **388**, 17 (2007)
- 9 J.A. McGuire, Y.R. Shen, *Science* **313**, 1945 (2006)
- 10 M. Smits, A. Ghosh, M. Sterrer, M. Mueller, M. Bonn, *Phys. Rev. Lett.* **98**, 098302 (2007)
- 11 S. Das, C. Ghosh, S. Gangopadhyay, U. Chatterjee, C.G. Bhar, V. Voevodin, O.G. Voevodina, *J. Opt. Soc. Am. B* **23**, 282 (2006)
- 12 R. Kaindl, M. Wurm, K. Reimann, P. Hamm, M. Weiner, A.M. Woerner, *J. Opt. Soc. Am. B* **17**, 2086 (2000)
- 13 S.H. Shim, D.B. Strasfeld, E.C. Fulmer, M.T. Zanni, *Opt. Lett.* **31**, 838 (2006)
- 14 T. Witte, D. Zeidler, D. Proch, K.L. Kompa, M. Motzkus, *Opt. Lett.* **27**, 131 (2002)
- 15 S. Ashihara, N. Huse, A. Espagne, E.T.J. Nibbering, T. Elsaesser, *J. Phys. Chem. A* **111**, 743 (2007)
- 16 C.W. Luo, K. Reimann, M. Woerner, T. Elsaesser, R. Hey, K.H. Ploog, *Phys. Rev. Lett.* **92**, 047402 (2004)
- 17 G. Ma, H.C. Allen, *Langmuir* **22**, 5341 (2006)
- 18 D.K. Hore, J.L. King, F.G. Moore, D.S. Alavi, M.Y. Hamamoto, G.L. Richmond, *Appl. Spectrosc.* **58**, 1377 (2004)
- 19 A.A. Mani, Z.D. Schultz, A.A. Gewirth, J.O. White, Y. Caudano, C. Humbert, L. Dreesen, P.A. Thiry, A. Peremans, *Opt. Lett.* **29**, 274 (2004)
- 20 E.W.M. van der Ham, Q.H.F. Vreken, E.R. Eliel, *Surf. Sci.* **368**, 96 (1996)
- 21 E.W.M. van der Ham, Q.H.F. Vreken, E.R. Eliel, *Opt. Lett.* **21**, 1448 (1996)
- 22 R. Braun, B.D. Casson, C.D. Bain, E.W.M. van der Ham, Q.H.F. Vreken, E.R. Eliel, A.M. Briggs, P.B. Davies, *J. Chem. Phys.* **110**, 4634 (1999)
- 23 L.J. Richter, T.P. Petralli-Mallow, J.C. Stephenson, *Opt. Lett.* **23**, 1594 (1998)
- 24 P. Hamm, M. Lim, W.F. DeGrado, R.M. Hochstrasser, *J. Chem. Phys.* **112**, 1907 (2000)
- 25 H. Maekawa, K. Tominaga, D. Podenas, *Japan. J. Appl. Phys.* **41**, L329 (2002)
- 26 H. Tsuji, *Macromol. Biosci.* **5**, 569 (2005)
- 27 C. Aleman, B. Lotz, J. Puiggali, *Macromolecules* **34**, 4795 (2001)
- 28 K. Aou, S.L. Hsu, *Macromolecules* **39**, 3337 (2006)
- 29 J.H. Hunt, P. Guyot-Sionnest, Y.R. Shen, *Chem. Phys. Lett.* **133**, 189 (1987)
- 30 S.H. Kang, S.L. Hsu, H.D. Stidham, P.B. Smith, M.A. Leugers, X.Z. Yang, *Macromolecules* **34**, 4542 (2001)